Article

Tuning Monte Carlo Models to Reproduce Cosmic Radiation Interacting with the Earth's Atmosphere

Muhammad Ajaz [1] , **Abd Haj Ismail** [2,3,*] , **Muhammad Waqas** [4] , **Ramoona Shehzadi** [5] , **Ishrat Asghar** [6] , **Hannan Younis** [7] , **Mateen Ullah Mian** [8] , **Atef AbdelKader** [2,3] , **Muhammad Adil Khan** [8] and **Kashif Safeen** [1]

[1] Department of Physics, Abdul Wali Khan University Mardan, Mardan 23200, Pakistan
[2] College of Humanities and Sciences, Ajman University, Ajman P.O. Box 346, United Arab Emirates
[3] Nonlinear Dynamics Research Center (NDRC), Ajman University, Ajman P.O. Box 346, United Arab Emirates
[4] School of Mathematics, Physics and Optoelectronic Engineering, Hubei University of Automotive Technology, Shiyan 442002, China
[5] Department of Physics, University of the Punjab, Lahore 54590, Pakistan
[6] Department of Physics, Faisalabad Campus, University of Education Lahore, Faisalabad 38850, Pakistan
[7] Department of Physics, COMSATS University Islamabad, Islamabad 44000, Pakistan
[8] Department of Physics, Islamia College Peshawar, Peshawar 25120, Pakistan
* Correspondence: a.hajismail@ajman.ac.ae

Abstract: In this work, we performed a comparative study between HIJING, Sibyll, and QGSJET model-based event generators. Such Monte Carlo (MC) models are used to simulate the interaction and propagation of high-energy cosmic radiation (e.g., coming from the sun) with the Earth's atmosphere. The global event observables selected for the study were the transverse momentum (p_T) spectra and rapidity density distributions of strange particles (K_S^0, Λ, and Ξ^-). This study was performed in the STAR and CMS fiducial phase spaces by simulating the strange particles in pp collisions at $\sqrt{s}$ = 200 GeV, 900 GeV, and 7 TeV, and the simulations were then compared to the experimental measurements. It was observed that none of the discussed model-based event generators ultimately predicted the experimental results, except QGSJET, which generally agrees reasonably with the data. However, QGSJET does not produce Ξ particles; therefore, it does not provide any predictions for Ξ. The other two models reproduced the data only in a limited rapidity or transverse momentum region while mainly underpredicting the data in the rest of the areas. These cosmic radiation simulation models are capable of covering the mid-rapidity regions of density distributions. Utilizing model-based observations, some fundamental parameters can be re-tuned and extrapolations to the highest energies can be investigated. Furthermore, these observations can provide valuable insights that could potentially constrain and improve perturbative- and non-perturbative-based QCD event generators, thereby facilitating a better understanding of the underlying physics.

Keywords: cosmic radiations; kinematic distribution; LHC energies; transverse momentum spectra

1. Introduction

High-energy cosmic ray particles are considered the most energetic particles observed in nature, and they originate from inside and outside our galaxy. They enter the top of Earth's atmosphere and interact with air molecules, and develop to create a cascade of secondary particles that reach the ground level. Generally, the secondary cascades are classified in three different parts: electromagnetic, muonic, and hadronic components. In the first interaction, daughter particles are produced, and they share the energy of the primary cosmic particle, and then continue to collide and further interact. These particles in the atmosphere are commonly called Extensive Air Showers (EAS) [1,2]. Furthermore, strange particles are among these created particles, such as kaons or lambda baryons, which are produced in the cascade of secondary particles initiated by the cosmic ray interactions. Moreover, the lifetimes of strange particles are relatively long, which enable

them to travel for longer distances in the atmosphere before decaying. This will give us the opportunity to study and learn more about their development and propagation in the atmosphere. In addition, as part of the cascades of secondary particles, the presence of strange particles contributes in the ongoing analyses of the energy and compositions of primary cosmic particles. Therefore, understanding these particles can play a key role in enhancing our knowledge about the nature and propagation of extensive air showers in the atmosphere, and therefore provide insights about the energy and type of primary cosmic particles. At energies above about 10–100 TeV, the flux of these particles is too small to be measured directly using direct cosmic ray experiments, such as balloon and satellite experiments [3,4]. Instead, large cosmic ray experiments are used to detect their energies indirectly [5,6]. Such experiments study the properties of secondary particles and their propagation in the atmosphere to obtain valuable information about the primary interacting cosmic particles at the top of the atmosphere. Therefore, Monte Carlo simulation models describe the interaction and propagation of these particles in the atmosphere. These models use Monte Carlo techniques, which involve generating random numbers to simulate the behavior of particles in a given system. Such simulation models can provide detailed information about the behavior of cosmic radiations, which is difficult to observe directly due to their high energy and the fact that they are constantly bombarding the Earth from all directions. By simulating the interactions of cosmic radiation with the atmosphere, the models provide insights into the production of secondary particles, which can be detected and used to study the properties of cosmic radiation. These models are valuable tools for studying the properties of cosmic radiation and developing new techniques for detecting it. The models simulate complex interactions between particles and the Earth's atmosphere, providing detailed information that would be difficult or impossible to obtain through direct observations.

One of the successes of modern physics is the extent to which strong interactions occurring in high-energy particle colliders can be accounted for with Quantum Chromodynamics (QCD), in particular, the short-distance partonic configurations and the production of heavy quarks and jets [7]. Both perturbative and non-perturbative (hard and soft QCD) processes determine the production of particles in high-energy colliders. Hard scattering processes with a large momentum transfer are understood in a perturbative Quantum Chromodynamics (pQCD) framework with the factorization theorem [8]. At low transverse momenta, particle production is dominated by parton hadronization. Soft processes can only be modeled with the help of phenomenological models and event generators for hadronic interactions. The experimental measurements from collider experiments provide constraints and information to tune the parameters of such hadronic and cosmic ray models [9].

Proton–proton (pp) collisions provide baseline measurements for heavy ion interactions and insights into the particle production mechanisms and serve as a valuable tool for tuning the parameters of hadronic Monte Carlo generators [10,11]. Since the initial states of colliding systems in high-energy colliders do not have strange content, information on the final strangeness production is crucial to study the properties of the strongly interacting medium created in high-energy collisions [12]. At high transverse momentum (p_T), the production of strange hadrons is dominated by flavor creation and excitation at the early evolution of high-energy collisions. The gluon splitting mechanism is mainly responsible for strangeness production during the subsequent stages. In string-fragmentation-inspired models, the strangeness production is suppressed due to the heavier mass of strange quarks [13,14] compared to u and d quarks in general. Insights gained from the studies of strangeness production in pp collisions at high-energy colliders prove essential for tuning hadronic Monte Carlo models [15]. Heavy ion collisions, on the other hand, involve the collision of two nuclei, that when colliding with the atmosphere, produce a shower of secondary particles that can be detected and studied. Such studies help understand the production and evolution of the QGP in astrophysical environments. Additionally,

heavy ion collisions in cosmic rays can provide information about cosmic ray sources and acceleration mechanisms, which remain an open question in astrophysics.

This work presents the strange particle's p_T spectra and rapidity density distributions from the pQCD-based Monte Carlo (MC) generator HIJING (Heavy Ion Jet INteraction Generator) and cosmic radiation air shower models QGSJETII and Sibyll in pp collisions at $\sqrt{s}$ = 200 GeV, 900 GeV, and 7 TeV. The models' initial versions are published in [16–18]. A detailed comparison of p_T and rapidity (y) distributions between simulations and experimental observations from the STAR and CMS experiments is presented. The experimental data recorded at 900 GeV and 7 TeV are scaled to the cumulative number of non-diffractive and double diffractive interactions, commonly known as non-single-diffractive (NSD) interactions [19,20]. The rapidity density distributions tell us the particle production in the phase space region of the detector. Rapidity distributions are also important for the investigations of longitudinal dynamics. Nuclear stopping, for example, is responsible for the differences in protons and anti-protons. For this case, hyperons depend on the initial baryon density, similar to protons. The relative rapidity distributions are expected to behave similarly for (anti-)hyperons and (anti-)protons [21].

It is worth mentioning that analyzing strange particles is important in the study of cosmic rays because they decay into muons detected on the Earth's surface. By analyzing the distribution and properties of these muons, one can infer important properties of the cosmic rays, such as their energy spectra and compositions. This study provides insights into the properties of cosmic rays and their sources. Furthermore, studying strange particles is vital for testing theories of fundamental physics, including the Standard Model. Strange particles provide an avenue for investigating the behavior of the strong forces at high energies and the properties of quarks and their interactions.

The manuscript is organized as follows: brief descriptions of the models are discussed in Section 2. Section 3 presents the findings and their corresponding analysis, while Section 4 summarizes the results.

2. Methodology and Models

The transverse momentum and rapidity spectra of strange hadrons K_s^0, Λ, $\bar{\Lambda}$, Ξ^-, and Ξ^+ in pp collisions at $\sqrt{s}$ = 200 GeV, 900 GeV, and 7 TeV estimated by the STAR [22] and CMS [23] experiments are presented here. These measured quantities from experiments are then benchmarked by simulating events using the HIJING1.38, Sibyll2.3d, and QGSJETII-04 models described below. For simplicity, the names HIJING, Sibyll, and QGSJETII are used throughout the manuscript. Many similar studies have been performed to study different observables, and details can be found in refs. [24–33].

HIJING combines the perturbative QCD-inspired models for the production of jet fragments with the Lund model [34] and the Dual Parton model [35] at medium energies ($\sqrt{s} \leq 20$ GeV/nucleon) for soft interactions of multi-string phenomenology at low p_T. Minijets are one of the important features of the HIJING Monte Carlo event generator. They are jets of high-energy particles that are created during the initial phase of high-energy heavy ion collisions. Minijets are thought to be produced by the fragmentation of partons (quarks and gluons) in the colliding nuclei. In HIJING, the production of minijets is modeled using a two-component model that includes soft and hard processes. The "string fragmentation" model describes the soft processes by modeling the production of low-momentum particles resulting from the breakup of color strings between quarks and gluons. The hard processes are modeled using perturbative QCD (pQCD), which describes the production of high-momentum particles in the fragmentation of partons. The HIJING Monte Carlo event generator uses a set of parameters to control the production of minijets, such as the minimum transverse momentum for jet production, the jet cone size, and the jet multiplicity. These parameters are tuned to match experimental data from heavy ion collisions [16,36]. The model uses both Pythia 5.3 and Jetset 7.2 to generate kinematical variables and jet fragmentation, respectively [37]. The HIJING model was mainly developed to explore the range of initial conditions that may appear in relativistic heavy ion collisions.

The nuclear shadowing effect for the functions of the parton structure is also included to observe the nuclear effects [38]. The HIJING model with tuned phenomenological parameters can retrace the behavior of data produced from pp multi-particles for a wide energy range ($\sqrt{s_{NN}}$ = 5–2000 GeV) [36].

The MC event generator Sibyll utilizes the Dual Parton Model (DPM), fragmentation Lund MC, and mini-jet model [39]. For soft interactions, Sibyll covers a comparatively bigger phase space. The Gribov–Regge element theory is implemented in this model for multiple scattering [40]. The model simulates the cascades of air showers and the flux of secondary particles produced due to the interaction of high-energy cosmic radiation in the atmosphere of Earth. The binding energies of nucleons do not affect high-energy interactions. For this reason, Sibyll describes the particle flow energy in the projectile direction and the production of particles at smaller angles [41]. Sibyll also partially retraces the general effects of leading particles, such as jet formation at high p_T. The updated version of Sibyll considers the effect of multiple interactions, the enhancement of leading ρ mesons, the increase in muon number, and the suppression of π^0 mesons by tuning the parameters of hadronization for the remnants and dissociation of diffraction as compared to the older versions. Charmed hadrons production is also included in Sibyll based on benchmarking with recent accelerator data [41].

QGSJET is an MC generator used to study the hadronic interactions and to interpret and analyze the data for the installation of numerous physics experiments [42]. QGSJETII relies on the theory of Gribov–Regge effective fields for the processes of multiple scattering [43]. The QGJETII model phenomenally incorporates each scattering process as "soft" and "semi-hard" pomeron exchanges. These pomerons share energy momentum between hard/soft parton processes and the inelastic fundamental interactions [44]. ThevQGSJETII model has been updated with the recent LHC data, and the latest version of QSJETII incorporates the production of charms, pair production of baryons, and beam remnants [37]. The model also works efficiently for cosmic ray physics interactions. QGSJETII includes mini jets at large energies to describe hard and soft scattering processes. It also deals with the multiple interactions and effects of saturation [42]. Moreover, the model exhibits a favorable consistency with the experimental data at elevated momenta, while at low momenta, the distributions are slightly overestimated [45]. Normally, the Monte Carlo models allow users to control the definition of unstable particles. In contrast to others, the QGSJET model does not allow controlling the decay of unstable particles by changing the parameters. In this model, such secondaries are forced to decay; therefore, only the products of such unstable particles are included as final state particles. Due to this reason, the QGSJET model cannot produce results in the case of Ξ baryon, and hence predictions of the QGSJET model are not shown for this particle [46].

3. Analyses, Findings, and Interpretation

Before going into the detail of the interpretations of the findings, it is worth mentioning that since a significant fraction of muons created as secondary cosmic rays originate from charged kaons [47], understanding the properties of kaons and their interactions with the atmosphere is crucial for accurately measuring and interpreting the properties of cosmic rays. In particular, the abundance and properties of strange particles can provide important clues about the sources and nature of cosmic rays and test fundamental physics theories.

Figure 1 shows the p_T spectra of K_S^0, $\Lambda(\overline{\Lambda})$, $\Xi^-(\overline{\Xi}^+)$ from pp collisions at $\sqrt{s}$ = 200 GeV compared with the model predictions. For simplification, the spectra can be explained at two different regions, low p_T; $0.25 < p_T < 2$ GeV/c, and high p_T; $p_T > 2$ GeV/c.
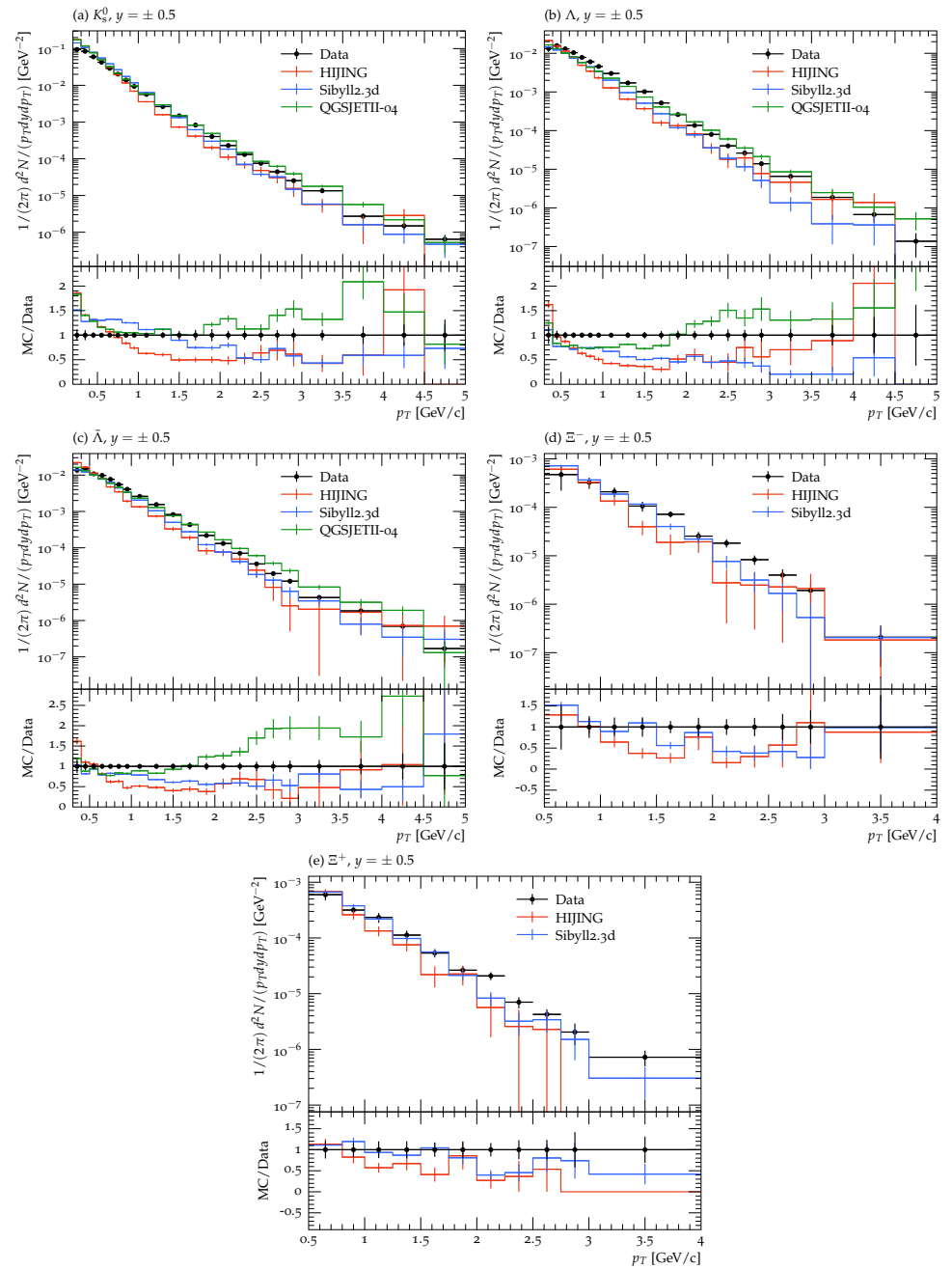
Figure 1. Transverse momentum p_T spectra simulated for (**a**) K_S^0, (**b**) Λ, (**c**) $\overline{\Lambda}$, (**d**) Ξ^-, and (**e**) Ξ^+ compared to the STAR measurements [22] at $\sqrt{s}$ = 200 GeV. Solid black dots are the experimental results, while the colored curves are model simulations. Additionally, the figure's lower panel presents the MC to data ratio.

In the case of K_S^0 shown in Figure 1a, no model describes the data completely at low p_T. The HIJING and QGSJET models overshoot the experimental observations up to $p_T \approx 0.7\,\text{GeV}/c$, while the Sibyll model overshoots up to 1 GeV/c. At $1.0 < p_T < 3.5$ and $p_T > 4.0\,\text{GeV}/c$, the QGSJET predictions are close to the experimental data within uncertainties but the model overpredicts at $3.5 < p_T < 4.0$. HIJING and Sibyll start to underestimate the data from $p_T \approx 0.8\,\text{GeV}/c$ and $\approx 1.5\,\text{GeV}/c$, respectively, and reproduce the data well above 3.5 GeV/c. For Λ and $\overline{\Lambda}$, the models reproduce the p_T spectra at very low p_T values of $< 0.6\,\text{GeV}/c$, except HIJING, which overpredicts by about 50% at p_T = 0.25. The Sibyll model underpredicts the experimental data by 15% up to $p_T \approx 1.3\,\text{GeV}/c$ and then underpredicts from $p_T > 1.3\,\text{GeV}/c$ by about 30 %. However, it reproduces the data

at $p_T > 3 \, \text{GeV}/c$ within the large uncertainties. However, HIJING underpredicts the data below $p_T \approx 3.5 \, \text{GeV}/c$ for Λ and $2.5 \, \text{GeV}/c$ for $\overline{\Lambda}$, respectively, but has good prediction afterward within the large experimental errors. The Sibyll model prediction is lower than the experimental data for $1.0 < p_T < 3.0$, but shows better prediction compared to the other two models on average over the entire p_T range. For $\Xi^- (\overline{\Xi}^+)$, at $p_T < 1.0 \, \text{GeV}/c$, the HIJING model can reproduce the experimental data within the estimated range of uncertainties; however, it tends to underestimate the data at higher p_T. Conversely, Sibyll can replicate the experimental data for p_T values less than $2 \, \text{GeV}/c$, but it falls short for $2 < p_T < 2.6$ in the case of Ξ^- and $2 < p_T < 2.3$ for $\overline{\Xi}^+$. Nevertheless, the model can reproduce the data afterwards within the estimated range of uncertainties. Furthermore, the models depict the decreasing trend of the differential yield of the particles with increasing p_T. The larger uncertainties in data and models are due to the small cross-section of these strange particles at 200 GeV. With the same statistics, the uncertainties are smaller at 900 and 7000 GeV due to their larger production cross-section.

The calculation and hence comparison of the mean transverse momentum ($< p_T >$) is essential when studying the p_T spectra in pp collisions. Figure 2 shows the $< p_T >$ of various particles calculated from the predictions of the models under study in pp collisions at $\sqrt{s}$ = 200, contrasted against the STAR measurements at RHIC [22]. It can be observed from the experimental data that $< p_T >$ tends to increase with the mass of particle species. The predictions of the QGSJET and Sibyll models reasonably match with the experimental data within the uncertainties and follow the increasing trend with particle mass. However, on the other hand, HIJING predictions are lower than the data but follow a similar increasing trend with particle mass. The dependence of $< p_T >$ on particle mass is due to the production of mini-jets in pp and $p\bar{p}$ collisions that contribute increasingly to the p_T spectra [48]. This contribution is expected to increase with the increasing mass of particle species [49]. The data and all three models depict this expanding effect of the p_T spectra with an increase in mass. Among the models, Sibyll has a better prediction than the other two, where QGSJET does not produce the short-lived particles as explained above.
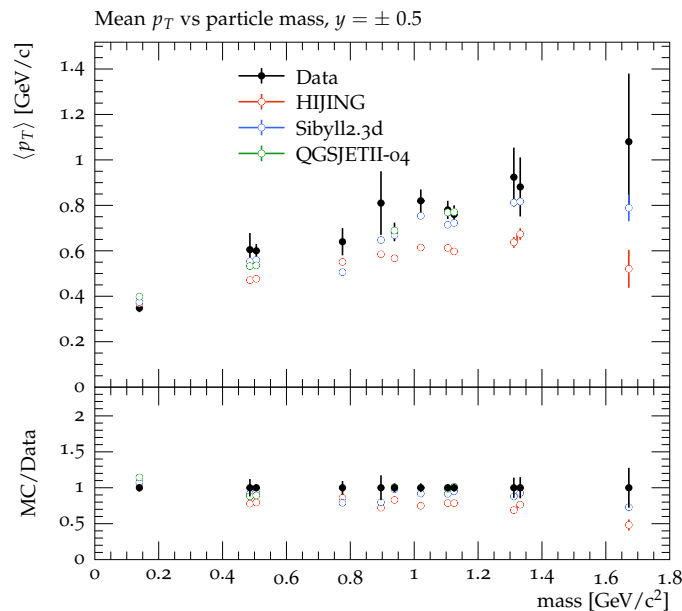

Figure 2. Mean p_T ($< p_T >$) as a function of particle mass at $\sqrt{s}$ = 200 GeV from STAR [22] compared to MC predictions in pp collisions. Solid black dots are experimental results and colored open markers are model simulations. The points from left to right represent the following particles: π, K_S^0 and K^-, ρ, K^*, $\bar{p}$, ϕ, Λ and $\bar{\Lambda}$, Ξ^- and Ξ^+, Ω^-. Additionally, the figure's lower panel presents the MC to data ratio.

Figure 3 (left column) shows the rapidity density distributions of (a) K_S^0, (c) Λ, and (e) Ξ^- in pp collisions at $\sqrt{s} = 0.9$ TeV [23]. Then, these distributions have been contrasted with the predictions of HIJING, Sibyll, and QGSJET. The MC to data (MC/data) ratio is presented in the lower panel of each plot. In the case of K_S^0, the HIJING model's predictions are the same as the experimental data within the uncertainty, while Sibyll and QGSJET undershoot the experimental measurements by up to 20%. The Sibyll model's predictions are better than QGSJET, particularly at the distribution's lower $|y|$ region, where the model reproduces the data within 10%. For Λ, none of the model's predictions describe the data. However, these models describe the shape of the distribution. QGSJET and HIJING predictions are lower than experimental data by about 20% and are the same compared to Sibyll, which underpredicts the data by about 25%. For Ξ^-, both Sibyll and HIJING undershoot the experimental results in all rapidity regions by about 35% and 30%, respectively.

Figure 3 (right column) shows the p_T spectra of (b) K_S^0, (d) Λ, and (f) Ξ^- in pp collisions at $\sqrt{s} = 0.9$ TeV [23] in comparison to the predictions of the different models under study. It has been observed that for K_S^0, all models have predictions closer to the experimental data for $p_T \sim 1$ GeV/c within the uncertainty, while they start to underpredict the data from $p_T > 1$ GeV/c. The predictions of the QGSJET model are closer to the experimental data than HIJING and Sibyll in the intermediate p_T regions, while Sibyll and HIJING have a better prediction at high p_T within the uncertainty. In the case of Λ p_T spectra, Sibyll reasonably reproduces the data up to $p_T < 4$ GeV/c, while the predictions of HIJING and QGSJET are lower at low p_T. However, the HIJING model produces good results at high p_T within the uncertainty. The Sibyll model overestimates the experimental data at high p_T regions, while the QGSJET underestimates the data. For Ξ^- p_T spectra, both HIJING and Sibyll underpredict the data by up to 50%. However, the shape of the spectra is described by these models.

Figure 4 (left column) shows the rapidity density distributions of (a) K_S^0, (c) Λ, and (e) Ξ^- in pp collisions at $\sqrt{s} = 7$ TeV [23]. These distributions are then compared with predictions of the HIJING, Sibyll, and QGSJET models. In the case of K_S^0, the HIJING model's predictions are the same as experimental data within uncertainty, except at $|y| = 1.5$, where the model slightly overshoots the experimental data. Sibyll and QGSJET undershoot the experimental measurements by about 10% and 15%, respectively. It has also been observed that the Sibyll and QGSJET start to converge at $|y| \approx 1.6$. For Λ, the QGSJET and HIJING models predict the experimental data within the large uncertainty. The Sibyll model, on the other hand, underpredicts the data by up to 40%. For Ξ^-, the Sibyll model undershoots the experimental results in all rapidity regions by about 40%. In contrast, the HIJING model describes the data within 10%, except at $|y| = 0.4$, where the model underpredicts by about 40%. Overall, all the studied models predicted the rapidity density distribution shapes well.

Figure 4 (right column) shows the p_T spectra of (b) K_S^0, (d) Λ, and (f) Ξ^- in pp collisions at $\sqrt{s} = 7$ TeV [23] in contrast with the theoretical forecasts of the different models under study. For K_S^0, the Sibyll model depicts the experimental data up to $p_T < 0.8$ GeV/c, but underpredicts the data for $0.8 < p_T < 6$ GeV/c. Above $p_T = 6$ GeV/c, the model reproduces the data within the experimental uncertainty. The HIJING model overshoots the data at $p_T < 0.7$ GeV/c, but underpredicts afterwards. The predictions of the QGSJET model are closer to the experimental data than HIJING and Sibyll for the $2 < p_T < 5$ GeV/c region. In contrast, the latter two models perform better in high p_T regions. In the case of Λ's p_T spectra, QGSJET reproduces the data at $p_T < 1$ GeV/c, but significantly underpredicts afterwards, having a greater discrepancy at higher p_T values. HIJING underpredicts for $1 < p_T < 4$ GeV/c and overpredicts in the lower and higher p_T regions. The Sibyll model underestimates the experimental data for the $p_T < 3.5$ GeV/c regions, but overpredicts at high p_T values. Overall, the spectral shape is described by the models. For the p_T spectra of Ξ^-, both HIJING and Sibyll do not reproduce the experimental data. However, the shape of the spectra is described by these models. The Sibyll model underpredicts the experimental

measurements in all p_T regions. The HIJING model overshoots the data for $p_T < 0.8\,\mathrm{GeV}/c$ but undershoots in the higher p_T regions.
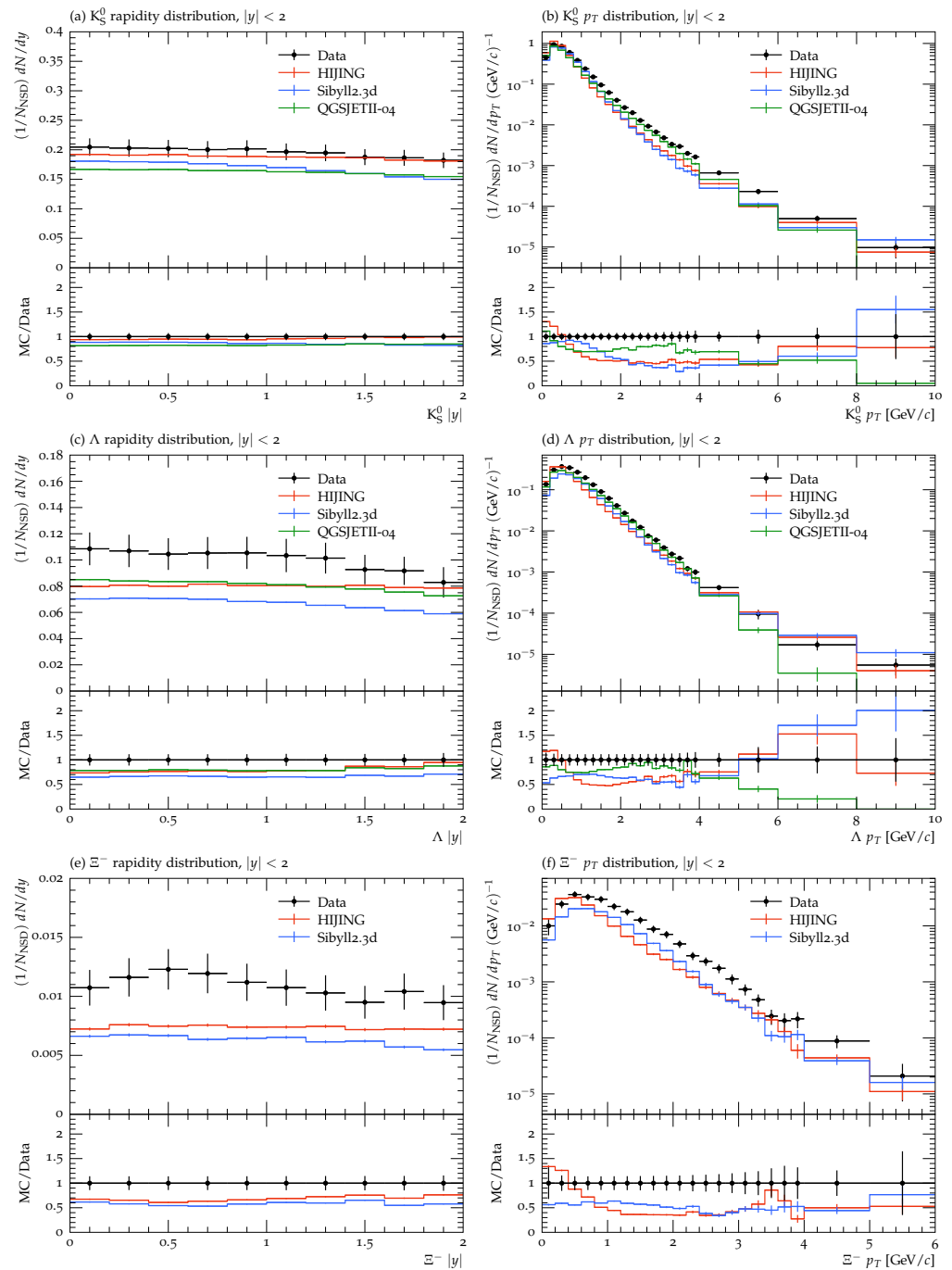

Figure 3. (**Left column**) The rapidity density distributions of (**a**) K_S^0, (**c**) Λ, and (**e**) Ξ^- and (**right column**) the p_T spectra of (**b**) K_S^0, (**d**) Λ, and (**f**) Ξ^- in pp collisions at $\sqrt{s} = 0.9$ TeV [23] in comparison with the predictions of the different models under study. The solid black dots are measurements, while the colored curves are model simulations. The lower panel of the graph gives the ratio of MC to the data.
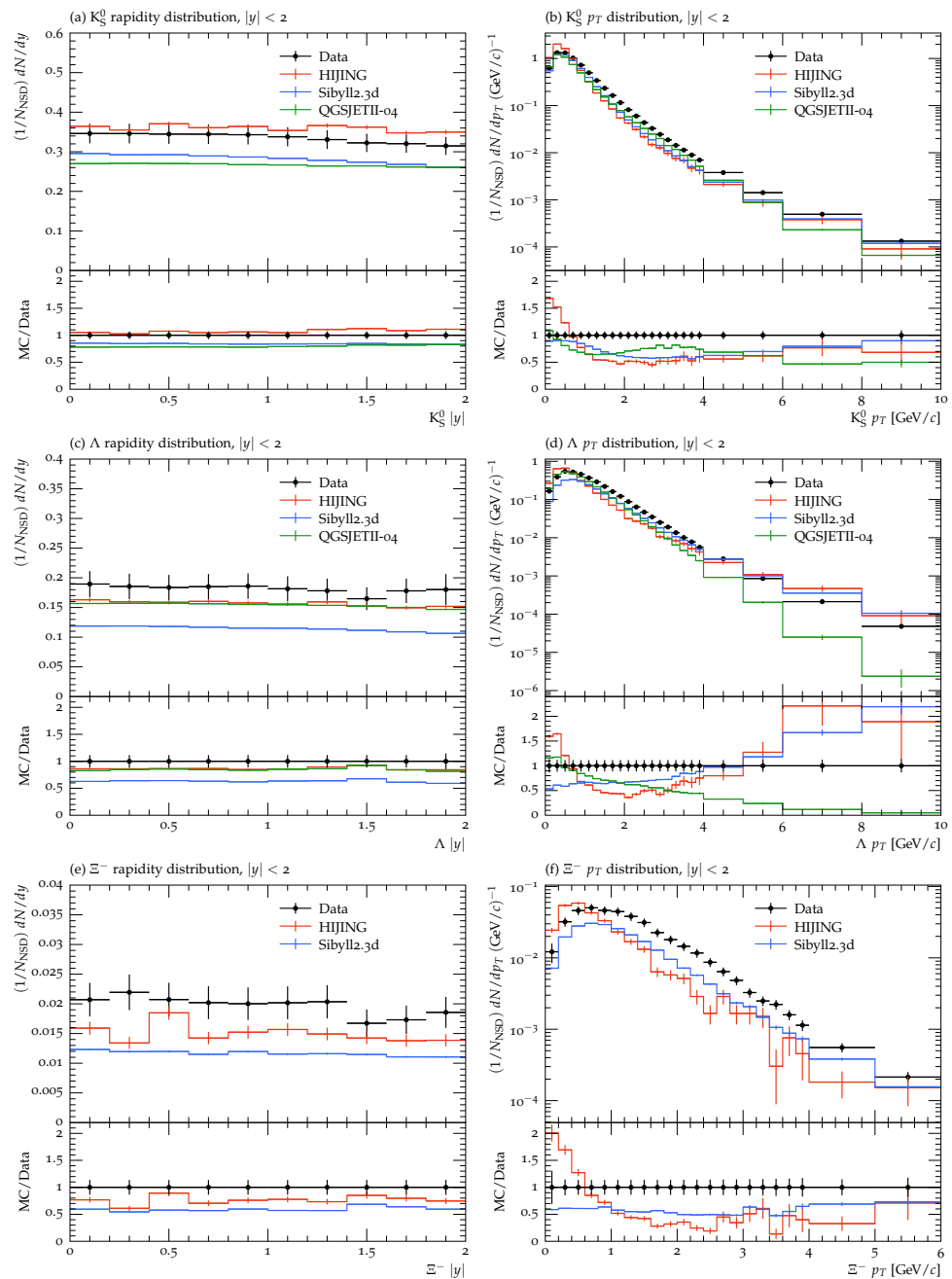
Figure 4. The (**left column**) shows the rapidity density distributions of (**a**) K_S^0, (**c**) Λ, and (**e**) Ξ^- and the (**right column**) shows the p_T spectra of (**b**) K_S^0, (**d**) Λ, and (**f**) Ξ^- in pp collisions at $\sqrt{s} = 7$ TeV [23] in comparison with the predictions of the models under study. The solid black markers are experimental data points and the different colored lines are model simulations. Additionally, the figure's lower panel presents the MC to data ratio.

4. Conclusions

This article presents a comparative study of Sibyll, HIJING, and QGSJET models with experimental data. The transverse momentum spectra and rapidity density distributions have been studied for various strange particles (K_S^0, Λ, and Ξ^-) in hadronic collisions at $\sqrt{s} = 200$, 900, and 7 TeV. The results reveal that none of the model predictions can entirely account for the experimental data concerning all the observables analyzed. The QGSJET and Sibyll models could reproduce the experimental data in a limited region of the p_T and $|y|$ distributions of the strange particles and failed to reproduce the particles' spectra for the kinematic range under study. However, HIJING predictions are in good agreement

only for K_S^0 rapidity density distributions at $\sqrt{s}$ = 900 GeV and 7 TeV, which can be explained by the strong color field effect included in this model. In hadron interactions at high energies, the production of strong color fields (strings) between the target and projectile partons is expected. In this framework, enhancements in the strange particles in such collisions have been reported to be explained by a strong longitudinal color field effect [50–55]. The discrepancy of the HIJING model in other distributions can be explained by the considerable pressure in the initial conditions; thus, large collective flow effects are not considered in this model. The HIJING model is similar to the QGSJET model in describing the observables for some particle distributions while reproducing similar predictions to Sibyll for others. The models have different predictions in the center and forward rapidity regions because the relative contributions of the production of particles are different in these regions. In the former case, hard pp interactions have a more significant contribution, resulting in events with high multiplicity and jets with high p_T. In the latter case, beam remnants and multiparton interactions (underlying events) are the main contributors. Since each process is governed by a different set of parameters in the event generators, each rapidity region requires different parameter tuning. While Sibyll and HIJING have been successful in many applications, their limited precision, underlying physics assumptions, limited tuning to collider data, and missing physics parameters can lead to underpredictions of the p_T values and rapidity distributions of strange hadrons in some cases. To reproduce better results, these models must be tuned with pre-and post-LHC data. In the current study, it is clear that these models have discrepancies in describing data at the RHIC and LHC energy scale, requiring further investigation.

References

1. Auger, P.; Ehrenfest, P.; Maze, R.; Daudin, J.; Robley, A.F. Extensive cosmic ray showers. *Rev. Mod. Phys.* **1939**, *11*, 288–291. [CrossRef]
2. Dorman, L. Cosmic Rays in the Earth's Atmosphere and Underground. In *Astrophysics and Space Science Library*; Springer: Dordrecht, The Netherlands, 2004; Volume 303. [CrossRef]
3. Seo, E.S.; Anderson, T.; Angelaszek, D.; Baek, S.J.; Baylon, J.; Buénerd, M.; Copley, M.; Coutu, S.; Derome, L.; Fields, B.; et al. Cosmic Ray Energetics Furthermore, Mass for the International Space Station (ISS-CREAM). *Adv. Space Res.* **2014**, *53*, 1451–1455. [CrossRef]
4. Adriani, O.; Barbarino, G.C.; Bazilevskaya, G.A.; Bellotti, R.; Boezio, M.; Bogomolov, E.A.; Bongi, M.; Bonvicini, V.; Bottai, S.; Bruno, A.; et al. The PAMELA Mission: Heralding a new era in precision cosmic ray physics. *Phys. Rept.* **2014**, *544*, 323–370. [CrossRef]
5. Aartsen, M.G.; Ackermann, M.; Adams, J.; Aguilar, J.A.; Ahlers, M.; Ahrens, M.; Alispach, C.; Andeen, K.; Anderson, T.; Ansseau, I.; et al. Cosmic ray spectrum and composition from PeV to EeV using 3 years of data from IceTop and IceCube. *Phys. Rev. D* **2019**, *100*, 082002. [CrossRef]
6. Scholten, O.; Pierre Auger Collaboration. Measurement of the cosmic-ray energy spectrum above 2.5×10^{18} eV using the Pierre Auger Observatory. *Phys. Rev. D* **2020**, *102*, 062005. [CrossRef]

7. Ellis, R.K.; Stirling, W.J.; Webber, B.R. QCD and collider physics. *Camb. Monogr. Part. Phys. Nucl. Phys. Cosmol.* **1996**, *8*, 1–435.
8. Collins, J.C.; Soper, D.E.; Sterman, G.F. Factorization of Hard Processes in QCD. *Adv. Ser. Direct. High Energy Phys.* **1989**, *5*, 1–91. ._0001. [CrossRef]
9. Adam, J. Pseudorapidity and transverse-momentum distributions of charged particles in proton–proton collisions at $\sqrt{s}$ = 13 TeV. *Phys. Lett. B* **2016**, *753*, 319–329. [CrossRef]
10. Ajaz, M.; Ahmed, A.; Wazir, Z.; Shehzadi, R.; Younis, H.; Khan, G.; Khan, R.; Ali, S.; Waqas, M.; Yang, P.P.; et al. Centrality dependence of PT distributions and nuclear modification factor of charged particles in Pb–Pb interactions at SNN = 2.76 TeV. *Results Phys.* **2021**, *30*, 104790. [CrossRef]
11. Ajaz, M.; Waqas, M.; Peng, G.X.; Yasin, Z.; Younis, H.; Haj Ismail, A.A.K. Study of pT spectra of light particles using modified Hagedorn function and cosmic rays Monte Carlo event generators in proton–proton collisions at $\sqrt{s}$ = 900 GeV. *Eur. Phys. J. Plus* **2022**, *137*, 52. [CrossRef]
12. Elia, D. Strange and identified particle production with ALICE at the LHC. *EPJ Web Conf.* **2015**, *95*, 03008. [CrossRef]
13. Waqas, M.; Peng, G.; Liu, F.-H. An evidence of triple kinetic freezeout scenario observed in all centrality intervals in Cu-Cu, Au-Au and Pb-Pb collisions at high energies. *J. Phys. G Nucl. Part. Phys.* **2021**, *48*, 075108. [CrossRef]
14. Muhammad, W.; Liu, F.-H.; Wang, R.-Q.; Irfan, S. Energy scan/dependence of kinetic freeze-out scenarios of multi-strange and other identified particles in central nucleus-nucleus collisions. *Eur. Phys. J. A* **2020**, *56*, 188. [CrossRef]
15. ALICE Collaboration. Enhanced production of multi-strange hadrons in high-multiplicity proton-proton collisions. *Nat. Phys.* **2017**, *13*, 535–539. [CrossRef]
16. Wang, X.N.; Gyulassy, M. HIJING: A Monte Carlo model for multiple jet production in pp, pA, and AA collisions. *Phys. Rev. D* **1991**, *44*, 3501. [CrossRef] [PubMed]
17. Kalmykov, N.N.; Ostapchenko, S.S.; Pavlov, A.I. EAS and a quark-gluon string model with jets. *Bull. Russ. Acad. Sci. Phys.* **1994**, *58*, 1966.
18. Fletcher, R.S.; Gaisser, T.K.; Lipari, P.; Stanev, T. SIBYLL: An event generator for simulation of high energy cosmic ray cascades. *Phys. Rev. D Part. Fields* **1994**, *50*, 5710–5731. [CrossRef]
19. Demir, D.A.; CMS Collaboration. Transverse-momentum and pseudorapidity distributions of charged hadrons in pp collisions at $\sqrt{s}$ = 0.9 and 2.36 TeV. *J. High Energy Phys.* **2010**, *02*, 041.
20. Khachatryan, V.; Sirunyan, A.M.; Tumasyan, A.; Adam, W.; Bergauer, T.; Dragicevic, M.; Erö, J.; Fabjan, C.; Friedl, M.; Fruehwirth, R.; et al. Transverse-momentum and pseudorapidity distributions of charged hadrons in pp collisions at $\sqrt{s}$ = 7 TeV. *Phys. Rev. Lett.* **2010**, *105*, 022002. [CrossRef]
21. Bruno, G.E. Rapidity distributions of strange particles in Pb-Pb at 158-A-GeV/c. *arXiv* **2005**, arXiv:nucl-ex/0511022.
22. Cadman, R.V.; Krueger, K.; Spinka, H.M.; McClain, C.J.; Underwood, D.G.; Abelev, B.I.; Adams, J.; Aggarwal, M.M.; Ahammed, Z.; Amonett, J. Strange particle production in p+p collisions at s**(1/2) = 200-GeV. *Phys. Rev. C* **2007**, *75*, 064901. [CrossRef]
23. Khachatryan, V.; Sirunyan, A.M.; Tumasyan, A.; Adam, W.; Bergauer, T.; Dragicevic, M.; Erö, J.; Fabjan, C.; Friedl, M.; Frühwirth, R.; et al. Strange Particle Production in *pp* Collisions at $\sqrt{s}$ = 0.9 and 7 TeV. *J. High Energy Phys.* **2011**, *05*, 64. [CrossRef]
24. Ajaz, M.; Bilal, M.; Ali, Y.; Suleymanov, M.K.; Khan, K.H. Models prediction of hadrons production ratios in pp collisions at $\sqrt{s}$ = 7 TeV. *Mod. Phys. Lett. A* **2019**, *34*, 1950090. [CrossRef]
25. Yang, P.P.; Ajaz, M.; Waqas, M.; Liu, F.H.; Suleymanov, M.K. Pseudorapidity dependence of the p_T spectra of charged hadrons in *pp* collisions at $\sqrt{s}$ = 0.9 and 2.36 TeV. *J. Phys. G* **2022**, *49*, 055110. [CrossRef]
26. Ajaz, M.; Haj Ismail, A.A.K.; Waqas, M.; Suleymanov, M.; AbdelKader, A.; Suleymanov, R. Pseudorapidity dependence of the bulk properties of hadronic medium in pp collisions at 7 TeV. *Sci. Rep.* **2022**, *12*, 8142. [CrossRef]
27. Tabassam, U.; Ali, Y.; Suleymanov, M.; Bhatti, A.S.; Ajaz, M. The production of pi (+/-), K-+/-, p and (p) over-bar in p-Pb collisions at root S-NN = 5.02 Tev. *Mod. Phys. Lett. A* **2018**, *33*, 1850094. [CrossRef]
28. Ajaz, M.; Waqas, M.; Li, L.L.; Tabassam, U.; Suleymanov, M. Bulk properties of the medium in comparison with models' predictions in pp collisions at 13 TeV. *Eur. Phys. J. Plus* **2022**, *137*, 592. [CrossRef]
29. Ajaz, M.; Khan, R.; Wazir, Z.; Khan, I.; Bibi, T. Model prediction of transverse momentum spectra of strange hadrons in pp collisions at $\sqrt{s}$ = 200 GeV. *Int. J. Theor. Phys.* **2020**, *59*, 3338 [CrossRef]
30. Khan, R.; Ajaz, M. Model predictions of charge particle densities and multiplicities in the forward region at 7 TeV. *Mod. Phys. Lett. A* **2020**, *35*, 2050190 [CrossRef]
31. Ajaz, M.; Tufail, M.; Ali, Y. Study of the production of strange particles in proton–proton collisions at $\sqrt{s}$ = 0.9 TeV. *Arab. J. Sci. Eng.* **2020**, *45*, 411–416. [CrossRef]
32. Haj Ismail, A. Monte Carlo simulation of the cosmic muon charge ratio. *Kuwait J. Sci.* **2022**, *49*, 1–8. [CrossRef]
33. Li-Li, L.; Ismail, A.H. Study of Bulk Properties of Strange Particles in Au+Au Collisions at $\sqrt{s_{NN}}$ = 54.4 GeV. *Entropy* **2022**, *24*, 1720. [CrossRef]
34. Andersson, B.; Gustafson, G.; Ingelman, G.; Sjöstr, T. Parton fragmentation and string dynamics. *Phys. Rep.* **1983**, *97*, 31. [CrossRef]
35. Capella, A.; Sukhatme, U.; Tran Thanh Van, J. Soft multihadron production from partonic structure and fragmentation functions. *Z. Phys. C* **1980**, *3*, 329. [CrossRef]
36. Soleiman, M.H.M. Event by Event Studies of Au-Au Collisions at $\sqrt{s_{NN}}$ = 200 GeV Using Two Event Generators. *Arab J. Nucl. Sci. Appl.* **2020**, *53*, 46–57. [CrossRef]

37. Ullah, S.; Ajaz, M.; Wazir, Z.; Ali, Y.; Khan, K.H.; Younis, H. Hadron production models' prediction for p T distribution of charged hadrons in pp interactions at 7 TeV. *Sci. Rep.* **2019**, *9*, 11811. [CrossRef]
38. Gyulassy, M.; Wang, X.N. HIJING 1.0: A Monte Carlo program for parton and particle production in high energy hadronic and nuclear collisions. *Comput. Phys. Commun.* **1994**, *83*, 307–331. [CrossRef]
39. Durand, L.; Hong, P. QCD and rising cross sections. *Phys. Rev. Lett.* **1987**, *58*, 303. [CrossRef]
40. Good, M.L.; Walker, W.D. Diffraction Dissociation of Beam Particles. *Phys. Rev.* **1960**, *120*, 1857. [CrossRef]
41. Riehn, F.; Engel, R.; Fedynitch, A.; Gaisser, T.K.; Stanev, T. Hadronic interaction model Sibyll 2.3 d and extensive air showers. *Phys. Rev. D* **2020**, *102*, 063002. [CrossRef]
42. Ostapchenko, S. Monte Carlo treatment of hadronic interactions in enhanced Pomeron scheme: QGSJET-II model. *Phys. Rev. D* **2011**, *83*, 014018. [CrossRef]
43. Baker, M.; Ter-Martirosyan, K.A. Gribov's Reggeon calculus: Its physical basis and implications. *Phys. Rept.* **1976**, *28*, 1. [CrossRef]
44. Ostapchenko, S. QGSJET-II: Towards reliable description of very high energy hadronic interactions. *Nucl. Phys. B-Proc. Suppl.* **2006**, *151*, 143–146. [CrossRef]
45. Ullah, S.; Ajaz, M.; Ali, Y. Spectra of strange hadrons and their role in neutrinos flux prediction. *EPL* **2018**, *123*, 31001. [CrossRef]
46. Calcagni, L.; Canal, C.G.; Sciutto, S.J.; Tarutina, T. LHC updated hadronic interaction packages analyzed up to cosmic-ray energies. *Phys. Rev. D* **2018**, *98*, 083003. [CrossRef]
47. Gaisser T.K. *Cosmic Rays and Particle Physics*; Cambridge University Press: Cambridge, UK, 1990.
48. Dumitru, A.; Spieles, C. Inverse slope systematics in high-energy p+p and Au+Au reactions. *Phys. Lett. B* **1999**, *446*, 326–331. [CrossRef]
49. Wang, X.N.; Gyulassy, M. A Systematic study of particle production in *p* + *p* (anti-p) collisions via the HIJING model. *Phys. Rev. D* **1992**, *45*, 844–856. [CrossRef]
50. Biro, T.S.; Nielsen, H.B.; Knoll, J. Colour rope model for extreme relativistic heavy ion collisions. *Nucl. Phys. B* **1984**, *245*, 449. [CrossRef]
51. Bialas, A.; Czyz, W. Chromoelectric flux tubes and the transverse-momentum distribution in high-energy nucleus-nucleus collisions. *Phys. Rev.* **1985**, *31*, 198. [CrossRef]
52. Gyulassy, M.; Iwazaki, A. Quark and gluon pair production in SU (N) covariant constant fields. *Phys. Lett. B* **1985**, *165*, 157. [CrossRef]
53. Merino, C.; Pajares, C.; Ranft, J. Effects of interaction of strings in the dual parton model. *Phys. Lett. B* **1992**, *276*, 168. [CrossRef]
54. Levai, P.; Skokov, V. Nonperturbative enhancement of heavy quark-pair production in a strong SU(2) color field. *Phys. Rev. D* **2010**, *82*, 074014. [CrossRef]
55. Hebenstreit, F.; Alkofer, R.; Gies, H. Pair Production Beyond the Schwinger Formula in Time-Dependent Electric Fields. *Phys. Rev. D* **2008**, *78*, 061701. [CrossRef]